Studies of microstructural changes upon retrogression and reaging (RRA) treatment to 8090 Al–Li–Cu–Mg–Zr alloy

K. S. Ghosh, K. Das and U. K. Chatterjee

Microstructural changes upon retrogression, and retrogression and reaging (RRA) treatment to 8090 Al–Li–Cu–Mg–Zr alloy in the peak aged (T8) temper have been studied by XRD and TEM. The variation of hardness with retrogression, and retrogression and reaging (RRA) has been measured to assess RRA behaviour. XRD studies exhibited all the phases that would be expected in the system. Retrogression primarily caused dissolution of matrix strengthening δ' precipitates in the solution. Reaging the retrogressed state caused reprecipitation of the δ' precipitates in the matrix. Retrogression and reaging (RRA) treatments retained the strength of the conventional peak aged temper, but TEM observations revealed some microstructural changes, such as growth of δ, T_1 and S′ phases, reduction of the dislocation densities, and generation of more dislocation loops and helices. MST/6039

Keywords: Retrogression and reaging, 8090 alloy, Dislocation loops and helices, S′ (Al_2CuMg) and δ (AlLi) precipitates

Dr Ghosh is in the Department of Metallurgical Engineering, National Institute of Technology, Warangal 506 004 (ghosh@nitw.ernet.in), and Dr Das and Professor Chatterjee are in the Department of Metallurgical and Materials Engineering, Indian Institute of Technology, Kharagpur 721 302, India. *Manuscript received 17 November 2003; accepted 23 March 2004.*

Introduction

Aluminium base alloys containing lithium are of potential interest to the aerospace industry because of their significantly higher values of specific strength and modulus compared with conventional aluminium alloys.[1,2] However, Al–Li alloys have reduced ductility and poor fracture toughness, marked anisotropy of mechanical properties, particularly a non-recrystallised structure, and are also susceptible to environmentally induced cracking (EIC).[3–5]

Cina[6,7] developed a non-conventional two stage heat treatment process, known as retrogression and reaging (RRA). This treatment is applied to materials in the T6 or T8 condition and involves heating for a short time at a temperature above the artificial aging temperature but around the solvus line of the matrix strengthening precipitates, followed by reaging to a condition similar to that of the original T6 or T8 temper. It has been reported that employment of the RRA treatment to 7000 and 8000 series alloys gave increased resistance to stress corrosion cracking (SCC).[8–11] The improvement in SCC resistance is attributed to microstructural changes associated with the RRA treatment. The 8000 series Al–Li–Cu–Mg–Zr alloys constitute an age hardening system comprising coherent ordered δ' precipitates along with β' (Al_3Zr) coherent dispersoids as well as other precipitates of T_1, S′, etc. Kanno *et al.*[12] recommended that RRA treatment is effective in alloys containing coherent dispersoids. Therefore, RRA treatment applied to the 8000 series Al–Li–Cu–Mg–Zr alloy should also be effective in improving SCC resistance while maintaining the strength level to that of the peak aged temper.

Microstructural development during conventional artificial aging of the 8000 series alloys has been reported in detail.[13–18] The types of precipitates observed in this complex system comprise phases such as δ' (Al_3Li), δ (AlLi) S′ (Al_2CuMg), T_1 (Al_2CuLi) and β' (Al_3Zr), etc. Work has been reported on how RRA treatments affect microstructural changes and also EIC performances.[11,19,20] In the present work, the microstructure of 8090 Al–Li–Cu–Mg–Zr alloy of T8 temper, and the microstructural changes after retrogression and reaging (RRA) treatment is given to this 8090-T8 alloy have been examined.

Experimental

8090 alloy was obtained from the Defence Metallurgical Research Laboratory (DMRL), Hyderabad, India, in sheet form having a thickness of 2·8 mm. The alloy sheet had been solutionised at 530–535°C, water quenched, stretched 1·5–2·5%, followed by artificial aging at 170°C for 24 h, corresponding to the peak aged T8 temper. The chemical composition (wt-%) of the alloy is given in Table 1.

Coupons of approximate dimensions $10 \times 10 \times 2{\cdot}5$ mm to study hardness and for TEM and XRD observations, were obtained from the as received alloy sheet. Retrogression treatments were applied to all specimens of as received T8 temper in a vertical tube furnace in air. The retrogression temperatures were chosen above and below the matrix strengthening precipitate δ' solvus line of the Al–Li system.[21] Specimens were retrogressed for a precise time in the furnace, quenched into ice cold water, followed by isothermal and duplex reaging to the peak aged temper. The retrogression schedule applied to the specimens is given in Table 2.

Before retrogression and reaging treatment, the as received alloy sheet surfaces were ground to 100 μm minimum so as to remove the lithium and magnesium depleted zones and subsurface porosity zones developed during alloy solutionising, which was carried out at a temperature 530–535°C in air.[22] After RRA treatment surfaces were polished with up to 600 grit emery papers lubricated with kerosene oil and finally de-oiled. The hardness values were measured using a Vickers hardness

Table 1 Chemical composition (wt-%) of sample 8090 alloy

Alloy	Li	Cu	Mg	Zr	Fe	Si	Al
8090	2·29	1·24	0·82	0·12	0·09	0·044	Bal.

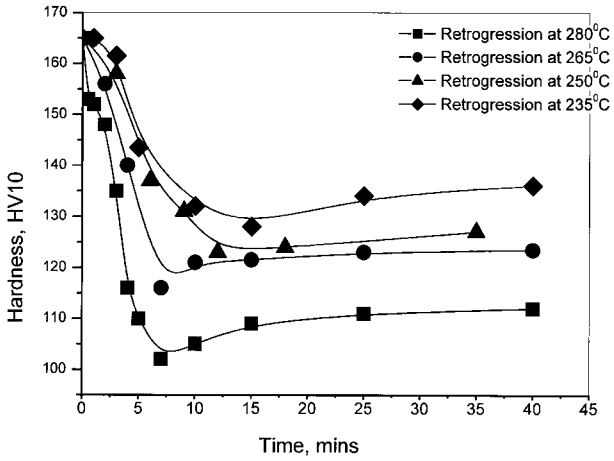

1 Hardness versus retrogression time for 8090-T8 sample

testing machine. X-ray diffraction (XRD) studies were carried out using a Philips PW 1710 diffractometer unit with cobalt and copper targets. For transmission electron microscopy (TEM) studies, samples were mechanically thinned to a thickness of approximately 100 μm, punched to obtain 3 mm discs and finally thinned to perforation using a Fischione twin jet electropolisher operating at 25 V and 2·5 A, in an electrolyte of composition 30%HNO_3 and 70%CH_3COOH at a temperature of approximately −20°C. A Philips CW12 transmission electron microscope was used for observation of the microstructures.

Results and discussion

RRA AND HARDNESS MEASUREMENT

Figure 1 shows plots of hardness versus retrogression time at retrogression temperatures of 235, 250, 265, and 280°C. The graphs exhibit the characteristic behaviour of retrogression phenomenon. The hardness versus retrogression time curves have two distinct regions: an initial sharp decrease in hardness; attainment of a minimum followed by a slight increase in hardness after which there is no further change in hardness values for the maximum retrogression time studied. The trends in the results are in agreement with the results for 7000 and 8000 series alloys obtained by other researchers.[23–25] However, the observed retrogression time corresponding to minimum hardness is different from that reported in other studies[19] as this depends on many variables, such as sheet thickness, heating medium, etc.[26] Further, the curves show that the higher the retrogression temperature the greater the drop in hardness and the shorter the retrogression time to attain minimum hardness.[24]

The variation in hardness of retrogressed and reaged material as a function of retrogression time is shown in Fig. 2. The figure indicates that reaging the retrogressed

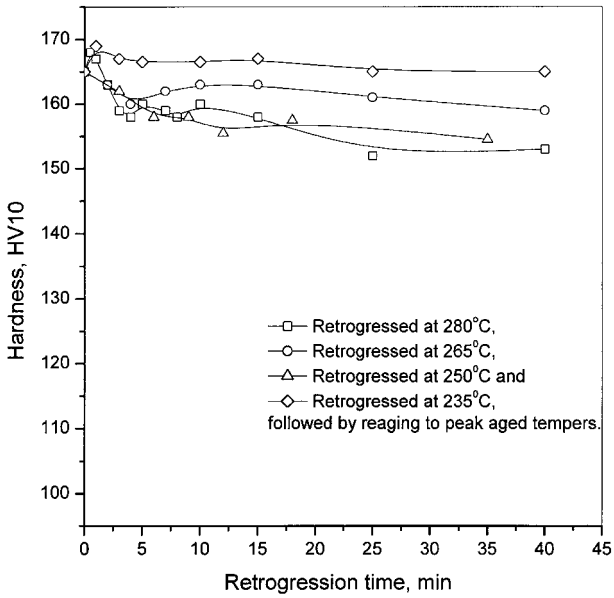

2 Variation of hardness with retrogression plus reaging to peak aged temper

temper caused the original peak hardness values to be approached. However, for the longer retrogression times, reaging to the peak aged temper failed to achieve the original peak aged hardness values. This is due to the fact that longer retrogression time at the retrogression temperature (it is to be noted that the retrogression temperature is quite high compared to that of the artificial peak aging temperature, 170°C) leads to a state of overaging temper.

Given the premise that the primary source of strengthening in the T8 condition is the presence of a coherent δ' phase, it is suggested that the initial decrease in hardness with retrogression time is due to preferential dissolution of shearable coherent matrix strengthening δ' precipitates, which are no longer stable at the retrogression temperature. During the retrogression process, other existing precipitates like T_1, S′, and S remain mostly undissolved (Fig. 7*a*, *b* and *c*), which is in agreement with work reported in the literature.[27] However, the growth of precipitates S′, T_1, and δ can occur to some extent (Fig. 3).[28] The decrease in dislocation density (*see* Fig. 11*b*)[11,19,29] during retrogression is also a contributing factor to the decrease in hardness. The minima in the retrogression curves are indicative of the maximum dissolution of δ' precipitates. At the time of minimum hardness, the rate of dissolution and the rate of reprecipitation of δ' precipitates may be equal and thereafter, beyond the hardness minimum, hardness may remain more or less constant with retrogression time. The greater decrease in hardness value with increase in retrogression temperature (Fig. 1) is attributed to the fact that a higher retrogression temperature causes more dissolution of δ' precipitates.[30] Further, the faster drop in hardness with

Table 2 Retrogression and reaging (RRA) schedule applied to sample 8090 alloy

Test	Retrogression temperature and time	Reaging schedule	RRA temper designation
Hardness	235, 250, 265 and 280°C for 1 to 40 min	Isothermal reaging (IA) at 170°C for 24 h corresponding to peak aging temper	...
XRD and TEM	250°C for 12 min	Isothermal reaging (IA) at 170°C for 24 h	8090R250IA
		Duplex aging (DA) at 150°C for 36 h, followed by heating to 195°C at a rate of 5–7 K min^{-1} and holding for 1 h at the temperature	8090R250DA
	280°C for 8 min	Isothermal reaging (IA) at 170°C for 24 h	8090R280IA
		Duplex aging (DA) at 150°C for 36 h, followed by heating to 195°C at a rate of 5–7 K min^{-1} and holding for 1 h at the temperature	8090R280DA

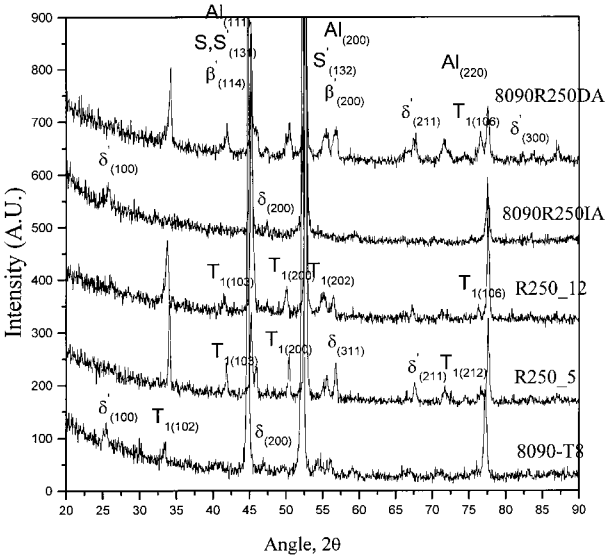

3 X-ray diffractograms of 8090 alloy at various tempers using Co K_α radiation

retrogression temperature requiring less retrogression time to minimum hardness, is consistent with the concept of faster dissolution kinetics with increasing temperature. Reaging the retrogressed tempers causes reprecipitation of the matrix strengthening δ' precipitates resulting in the (near) attainment of the original peak hardness values. Thus retrogression and reaging (RRA) tempers have hardness values approaching that of the conventional peak aged (T8) temper.

RRA AND X-RAY DIFFRACTOGRAMS

Figure 3 shows X-ray diffractograms of the as received 8090-T8 alloy, the alloy retrogressed at 250°C for different times (5 min and 12 min), and the alloy retrogressed and reaged (8090R50DDA and 8090R250IA).

Diffractograms at all tempers show peaks of all the probable phases that would be present in the alloy system, such as α-Al matrix, δ' (Al_3Li), δ (AlLi), S′ (Al_2CuMg), T_1 (Al_2CuLi), and β' (Al_3Zr) phases. Diffractograms (Fig. 3) of samples of 8090 alloy retrogressed at 250°C for 5 min and 12 min indicate the disappearance of the $\delta'_{(100)}$ peak and the appearance of an additional $T_{1(102)}$ peak and other intensified peaks of T_1 and δ phases. The appearance of the additional $T_{1(102)}$ peak and other intensified peaks of T_1 and δ phases is due to fact that with dissolution of δ' phase into solution during retrogression, the lithium content of the solid solution increases, resulting in the nucleation and growth (and also growth of the existing phases in the as received alloy) of lithium bearing phases. Diffractograms of the alloy retrogressed and reaged to peak hardness (RRA) show the reappearance of the $\delta'_{(100)}$ peak together with the presence of the other additional peaks from the T_1 and δ phases formed during retrogression.

MICROSTRUCTURES

In transmission electron microscopy (TEM) studies, attention has been focused on observing the second phase precipitates within the grains, and on the high angle and low angle grain boundaries. This has enabled an assessment of the changes in the size, distribution, and morphology of precipitates with the retrogression and reaging (RRA) treatment. Diffraction patterns of the phases have not been reported as these are well established for these alloy systems.[31–35]

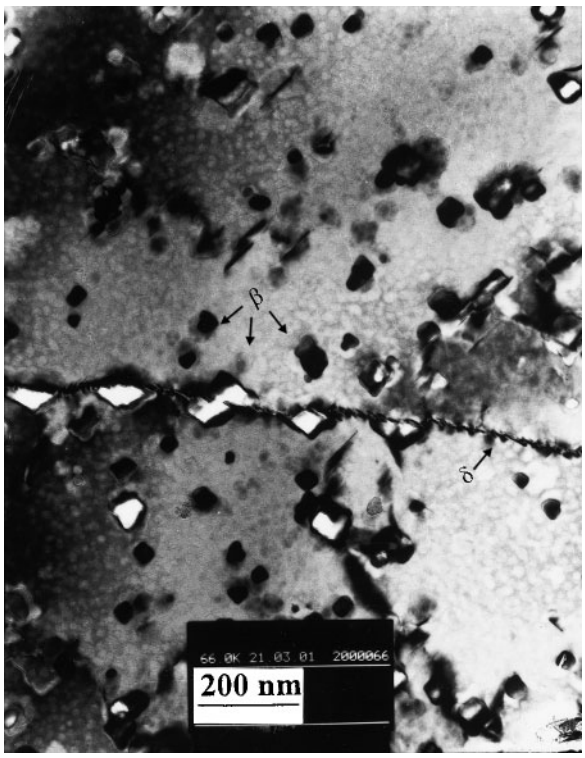

4 TEM image of 8090-T8 temper sample

β' (Al_3Zr) dispersoids

Figure 4 shows TEM photomicrographs of the 8090 alloy in the peak aged (T8) condition, and exhibits irregular shaped β' (Al_3Zr) dispersoids on high angle grain boundaries and in the matrix and δ.

The β' precipitates are stable owing to the low solid solubility of Zr in Al, small misfit, and sluggish zirconium diffusion.[36,37] The dispersion of these particles, size ranging from 20–30 nm diameter, is very effective in pinning grain and subgrain boundaries during thermal and mechanical processing, and thus inhibiting recrystallisation.[38] On the other hand, coherent β' (Al_3Zr) precipitates provide heterogeneous nucleation sites for matrix strengthening δ' (Al_3Li) phase. The reduction of both strain and surface energy is responsible for the effectiveness of the β' particles in nucleating δ' phase.[13,39] Indeed, they can induce precipitation at lithium levels that are inadequate for homogeneous nucleation.[40,41] In the present work β' (Al_3Zr) dispersoids acted as a heterogeneous nucleation site for some of the δ' precipitates, resulting in the formation of duplex δ' (i.e. δ' coated β') particles. Because of the high stability of the β' particles, the size and the distribution of particles will not be altered at the retrogression and reaging temperatures.

δ' (Al_3Li) precipitation

Figure 5*a*–*c* shows dark field images of the matrix strengthening δ' precipitates of the peak aged (T8), 8090R280IA and 8090R280DA tempers. Figure 6*a*–*c* gives a representation of the size of δ' particles and their distribution as histograms for the 8090-T8, 8090R280IA and 8090R280DA tempers. The δ' particle size distribution was analysed using Leica QWIN software and by selecting different regions of δ' images. The software has options for determining area fraction covered by the δ' precipitates, median, mean, standard deviation, kurtosis, skewness, etc., of the particle size distribution.

The volume fraction of δ' precipitates in different tempers can be calculated using the expression given by

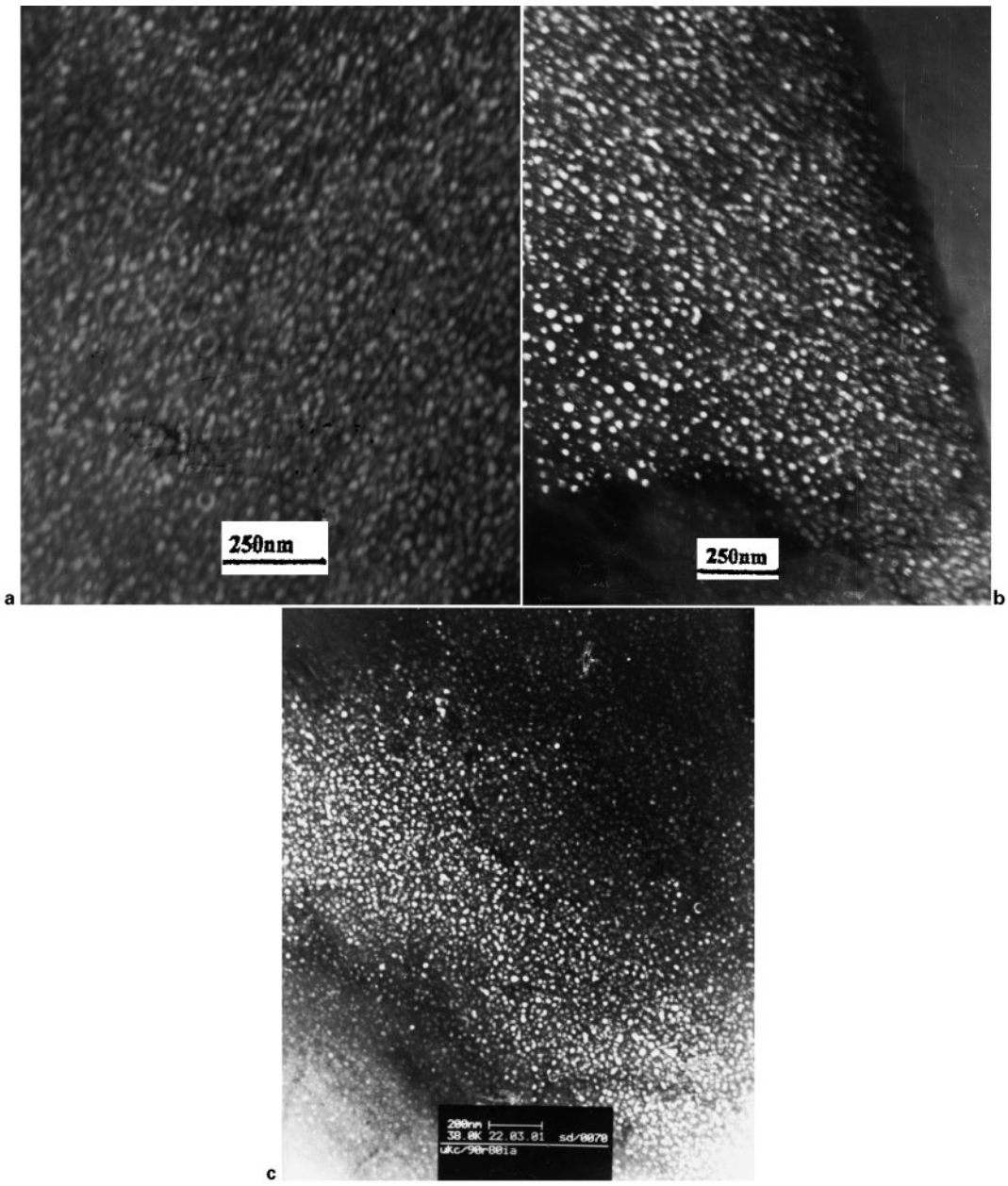

a 8090-T8; *b* 8090R280DA; *c* 8090280IA

5 Dark field image of δ' in samples having different tempers

Underwood[42] for spherical particles of diameter D

$$f'_{\delta} = -2\ln(1-A)D/(D+3t)$$

where A is the area fraction of the δ' particles as measured from the dark field TEM image, and t is the thickness of the foil. In the present calculation, the particle median has been used to determine the volume fraction. For volume fraction calculation, foil thickness has been taken to be 100–120 nm. The calculated volume fraction of δ' precipitates for different tempers are given in Table 3. The table indicates that the volume fraction of the δ' precipitates in the conventional peak aged and RRA tempers remains more or less the same. In this context, it is to be borne in mind that a variation in foil thickness of 20 nm results in about 10% variation in the calculated volume fraction of the precipitates.

The 8090 alloy in the retrogressed state was also studied using TEM, but no δ' phase was detected, indicating that all the δ' precipitate had been dissolved by the retrogression treatment.

S′ (Al_2CuMg) precipitation

Figure 7*a* shows rodlike and platelike (i.e. impinged rectangular rods along a line) S′ precipitates on dislocations that have been generated during stretching after solutionising, in the 8090-T8, temper. Similar observations have been reported by other investigators.[43,44] Irregular shaped β' particles are also visible in the micrograph.

The S′ (S) precipitation process in Al–Cu–Mg alloys has been discussed in the literature.[43,45,46] In ternary Al–Cu–Mg alloys, heterogeneous nucleation takes place on the high density of dislocation loops and helices that are present in the as quenched condition. But, in lithium containing alloys, the strong lithium atom vacancy binding energy inhibits vacancy condensation and formation of loops and helices: the only available heterogeneous nucleation sites are grain and subgrain boundaries. But, for appreciable S′ precipitation in quaternary Al–Li–Cu–Mg alloys, preaging stretching is required. In the 8090 alloy, 1·5–2·5% pre-aging stretching increases the dislocation density and these dislocation sites act as nucleation sites for the observed heterogeneous precipitation of S′ (S) precipitates[37] (Fig. 7*a*, *b* and *c*).

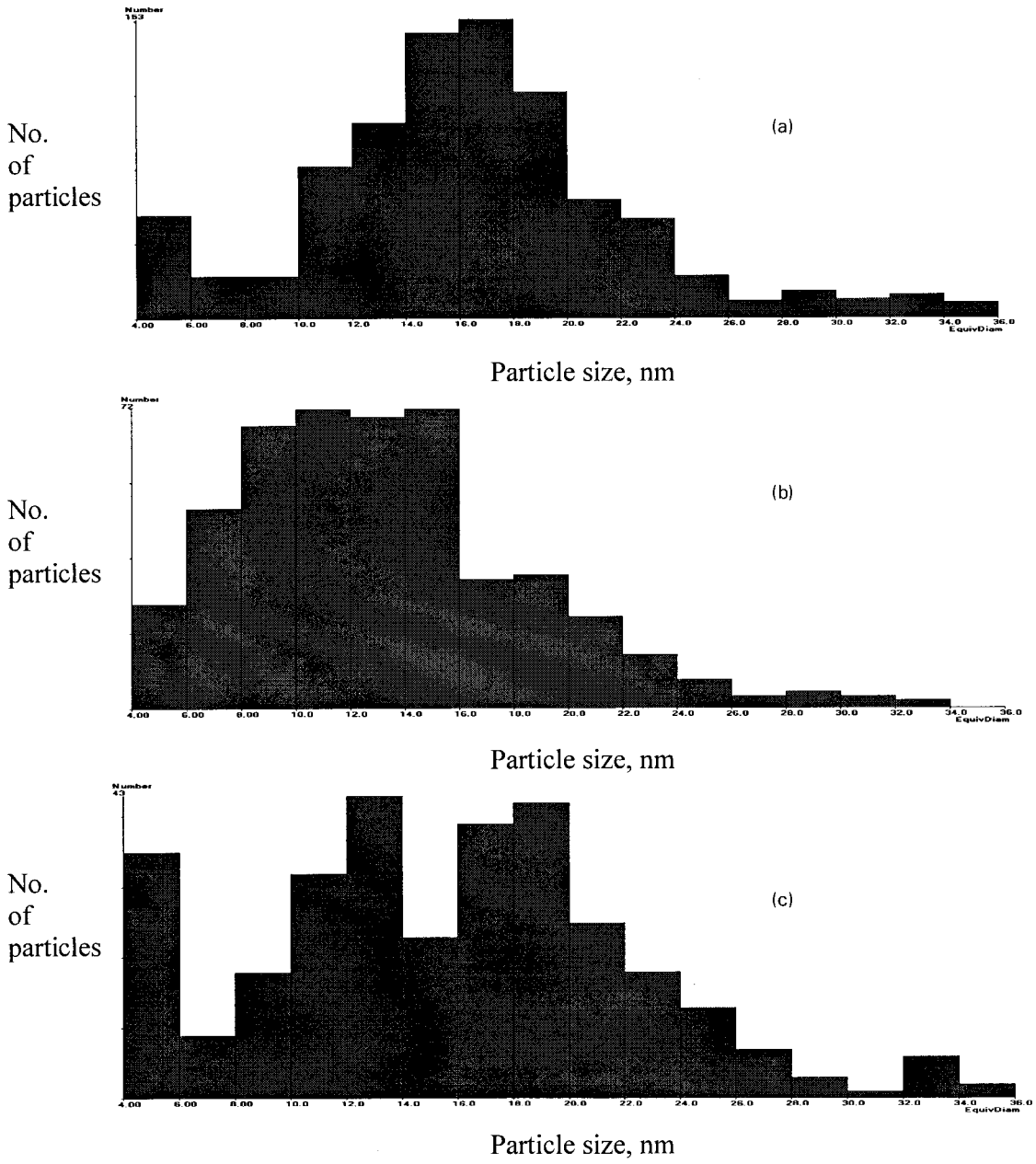

a 8090-T8; *b* 8090R280IA; *c* 8090R280DA

6 Histograms of δ' particle size and distribution in samples having different tempers

Figure 7*b*, *c* shows rodlike and platelike (i.e. impinged rectangular rods along a line) S′ precipitates on dislocation sites in 8090R280IA and 8090R250DA tempers. A similar type of S′ precipitates distribution was observed in the as received peak aged temper (Fig. 7*a*). Thus it is to be concluded that RRA treatment has not altered the existing distribution of S′ precipitates on the dislocations, i.e. retrogression treatment does not cause dissolution of S′ precipitates in the matrix.

Dislocation loops, helices and decoration of precipitates

Figure 8*a* shows the S′ and T_1 phases preferentially precipitated on dislocation and dislocation loops for the alloy in the T8 temper.[17,47,48] Figure 8*b*, *c* show S′ and T_1 phases preferentially precipitated on dislocation and dislocation loops as well as in the matrix in 8090R280IA and 8090R250IA tempers. The micrographs indicate that RRA treatment resulted in more dislocation loops and

Table 3 Details of δ' particles image analysis and estimated volume fraction of δ' particles

		Field 1: δ' particles image			Field 2: δ' particles image		
Alloy temper	Foil thickness *t*, nm	Area fraction	Median, nm	Volume fraction ($\times 10^{-3}$)	Area fraction	Median, nm	Volume fraction ($\times 10^{-3}$)
8090-T8	100–120	0·26	15·5	29–25	0·25	15·0	27–23
R280IA	100–120	0·27	13·34	27–23	0·29	13·0	27–24
R280DA	100–120	0·27	15·0	29–25	0·22	16·0	25–21

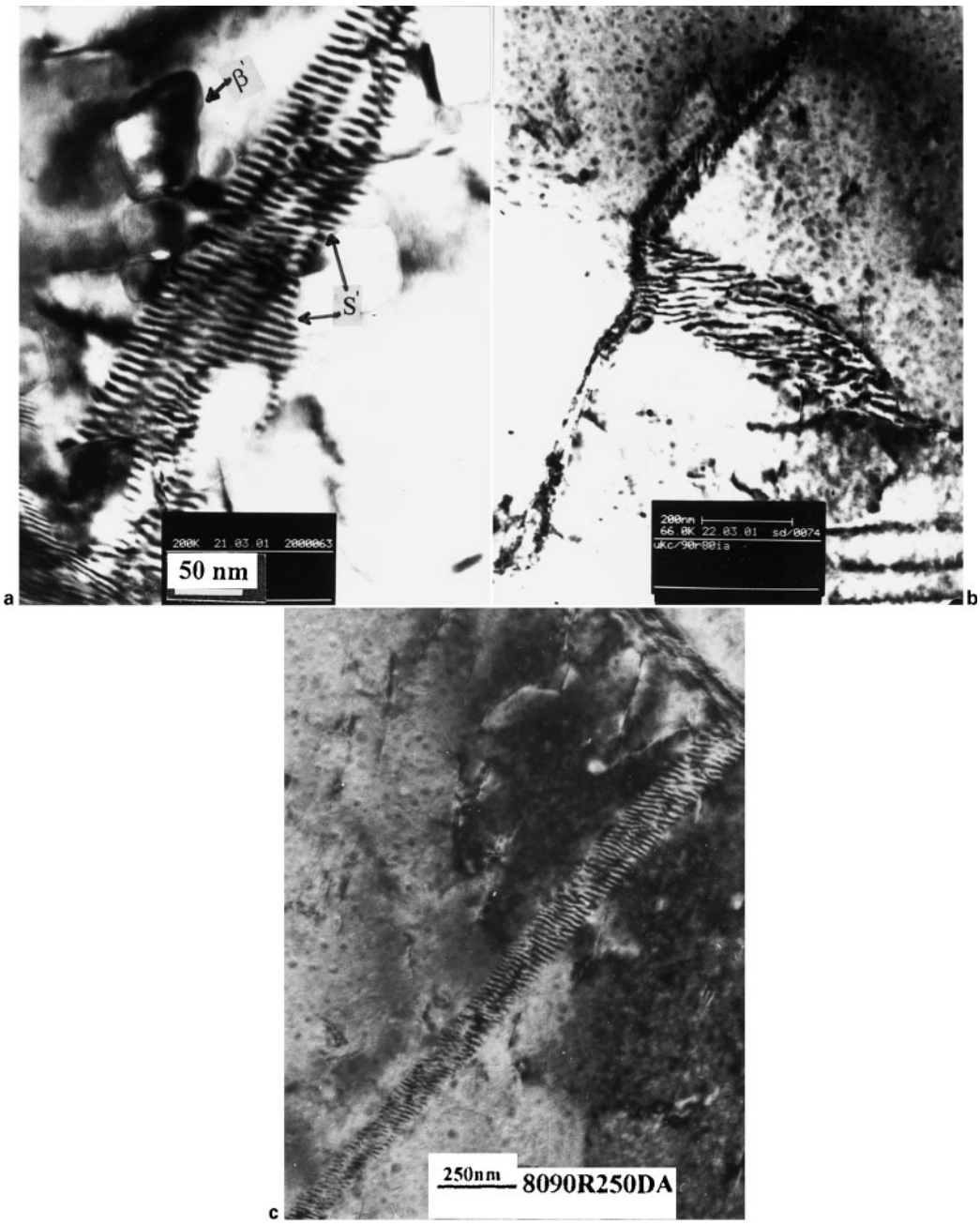

a 8090-T8; *b* 8090R280IA; *c* 8090R250DA

7 TEM images of S′ precipitates on dislocations in samples having different tempers

helices and additional precipitation of S′ and T_1 phases on these dislocations loops and helices. The generation of more dislocations loops and helices and precipitates in the RRA tempers (as observed in Fig. 8*b* and *c*) needs to be explained.

Retrogression causes the dissolution of δ' precipitates and GP zones that influences the vacancy concentration to the extent that vacancies are released by the dissolution of these zones. Like Mg, Li–vacancy binding energy in binary Al–Li alloy and ternary Al–Li–Zn alloys[49] has been reported to be high. Gregson *et al.*[15] claim that Li in solid solution in Al–Li–Cu–Mg alloys significantly reduces the free vacancy concentration due to its high vacancy binding energy, and that the precipitation and growth of δ' would therefore increase the concentration of free vacancies. This argument appears to contradict the hypothesis of Baumann and Williams[50] and Suzuki *et al.*[51] who maintain that the δ' phase acts as vacancy traps and confines them during aging. It is, however, possible for both these situations to exist in an alloy as follows: the formation of δ' will increase the free vacancy concentration, but there is a high probability for these free vacancies to encounter Li atoms in solid solution repeatedly (due to the high Li concentration in the alloy studied) before they can reach a matrix dislocation or grain boundary, get dragged by the Li atom back to the δ' precipitates, and thereby relieve Li supersaturation and permit δ' growth. In this sense, these 'free' vacancies are 'trapped' in the matrix, serving the function of repeatedly transporting Li to δ'. In the retrogression process, vacancy mobility will be affected by the increase in temperature from ambient to retrogression temperatures (250 and 280°C) as well as by the increased solutes content (Li, Mg, and Cu) in the solid solution, resulting from the complete dissolution of GP zones and δ'. Although these elements in solid solution are very effective in keeping vacancies bound at room temperature, they are not as effective at these higher

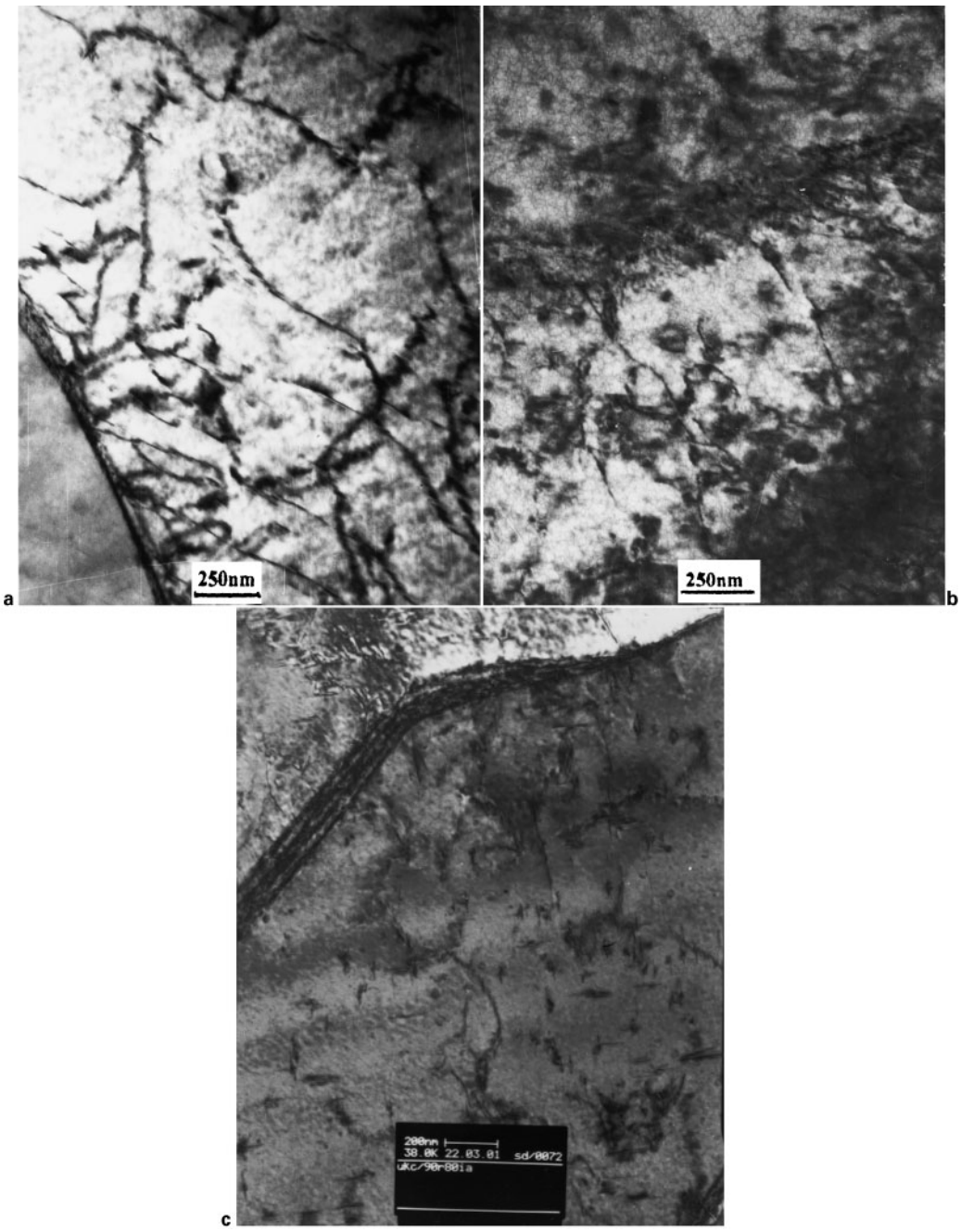

a 8090-T8; *b* 8090R250IA; *c* 8090R280IA

8 TEM images showing dislocation loops and helices containing T_1 and S′ precipitates in samples having different tempers

temperatures and a percentage of these vacancies will migrate to sinks such as grain boundaries and dislocations. Some of the vacancies can collapse into loops and helices and condense on existing loops and helices. These will have an impact on the distribution of the precipitates by providing nucleation sites for further strengthening phases during artificial aging.

Artificially reaging the retrogressed state results in the reprecipitation and growth of δ' phase. With increasing reaging time, the solid solution (i.e. matrix) becomes progressively diluted in Li, thereby enhancing further the vacancy mobility and lowering vacancy supersaturation. These vacancies can continue to form loops, migrate to dislocations, and form helices, or annihilate at grain boundary sinks. The first two mechanisms will provide additional nucleation sites for the strengthening phases within the matrix while the third one provides transport of solute atoms to grain and subgrain boundaries, thereby encouraging growth of S′ and T_1 at these sites.[17]

Uniform T_1 and S′ precipitation

Figure 9*a*, *b* show TEM micrographs of 8090R280DA tempers, which exhibit a uniform distribution of heterogeneous precipitation of T_1 and S′ phases within the matrix. The retrogression and reaging treatments have caused an increase in T_1 phase, which has also been reflected in the X-ray diffractograms of Fig. 3. This happens because during retrogression Li goes into solution, causing growth of Li bearing phases such as T_1 and δ phases. The retrogression and reaging treatments may also cause further S′ phase precipitation.[37] Homogeneous precipitation of S′ phase in 8090 alloy depends upon free vacancy concentration, and this is a function of both solution treatment

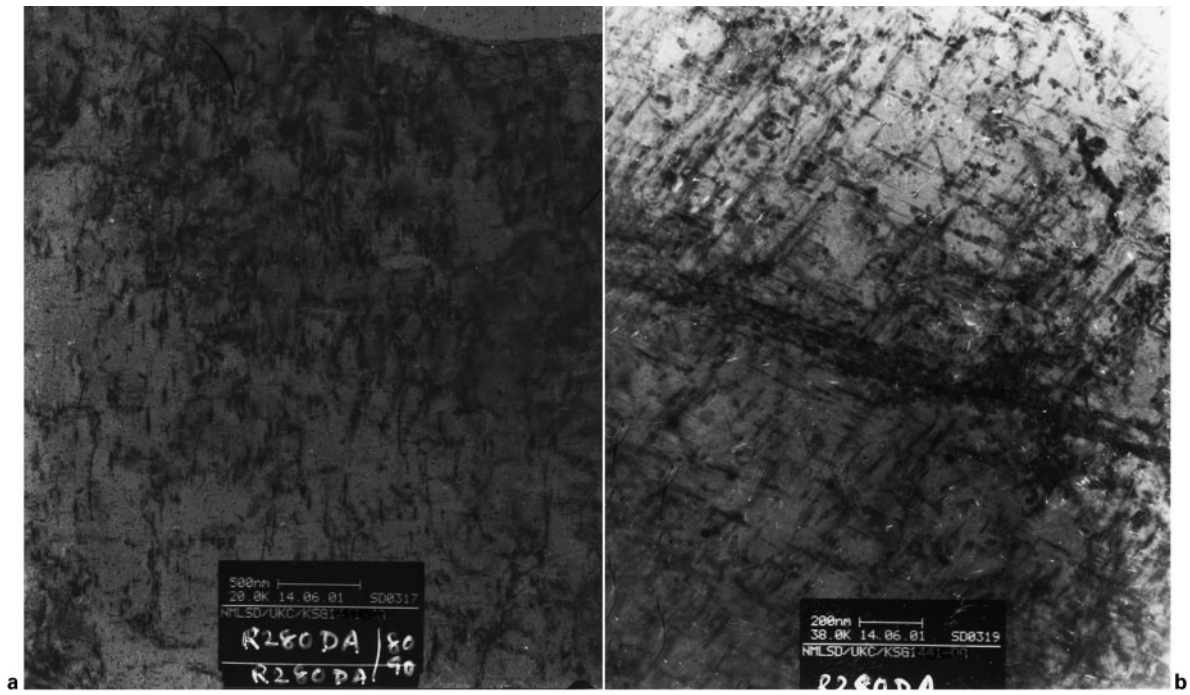

9 TEM images of 8090R280DA showing widespread distribution of T_1 and S′ precipitates in matrix

temperature and low temperature aging, before artificial aging at a higher temperature. During reaging of the retrogressed state at low temperature (150°C), nucleation and growth of δ' particles occur. During the growth of δ' phase, excess Cu and Mg concentration occurs at the growth front and also the vacancies strongly bound to Li atoms are released. Both of these effects lead to the development of a large volume fraction of S′ precipitates. There is enough evidence that the widespread homogeneous uniform distribution of S′ precipitates promotes cross-slip thereby dispersing slip resulting homogeneous deformation with an improved ductility and toughness.[37] Tensile tests have been carried out on the T8, four RRA, and over aged (T7) tempers at nominal strain rate ($\sim 1{\cdot}33 \times 10^{-3}\ s^{-1}$) as well as at low strain rate ($\sim 6{\cdot}0 \times 10^{-6}\ s^{-1}$) at room temperature and it has been found that there is an improvement in ductility values in the RRA tempers over the T8 temper.[48]

δ (AlLi) precipitation

Figure 10*a* is a TEM micrograph of the 8090R280IA RRA tempers showing equilibrium δ precipitates on the high angle grain boundaries. δ phase is also visible on the high angle grain boundaries as well as on the subgrain

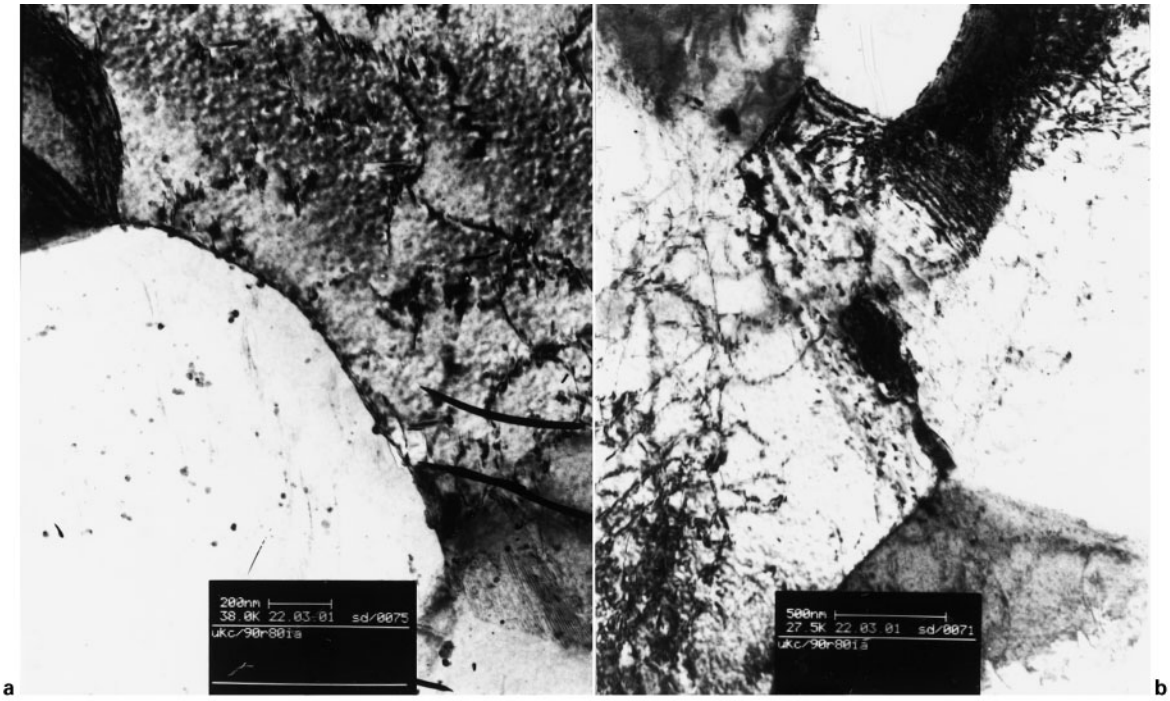

10 TEM images of 8090R280IA showing *a* equilibrium δ precipitates along high angle grain boundaries; and *b* δ precipitates along high angle grain boundaries as well as along subgrain boundaries

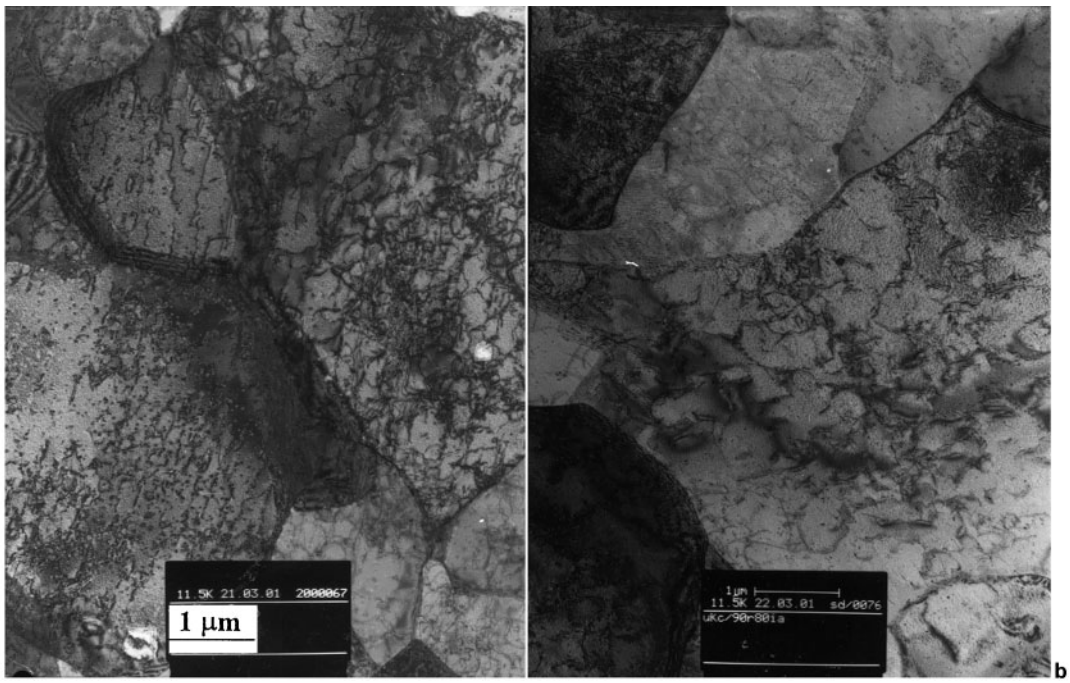

a 8090-T8; *b* 8090R280IA

11 Dislocation densities within the grains of two differently tempered samples

boundaries for the same RRA temper in Fig. 10*b*. The decoration of S′ and T_1 precipitates on stray dislocations are also visible. RRA treatments resulted in the formation of a large amount of δ phase and coarsening of the precipitates along the subgrain and grain boundaries, compared to that of the T8 temper (Figs. 4, 10*a* and 10*b*). Similar results after RRA are also reported in the literature.[9,12,52]

During retrogression, the dissolution of δ' phase increases lithium concentration in the solid solution and this causes the nucleation and growth of δ phase along subgrain and grain boundaries as well as the growth of the existing δ precipitates. Reaging the retrogressed state causes further growth of this phase. It is a well established fact that the longer the aging time the greater the amount of δ phase precipitation on high angle grain boundaries as well as on low angle boundaries. Since the total aging time in RRA is twice the aging time of the conventional peak aging temper, it is obvious that the microstructure of RRA treated alloy will contain a large volume fraction of coarse δ phase, so that the microstructure will approach that of the overaging (T7) temper. The precipitation of δ phase along low angle grain boundaries after long aging times was also observed by Tosten *et al.*[53] in Al–2Li–3Cu. It is to be mentioned that the additional coarse δ precipitation on high and low angle grain boundaries causes an improvement in the resistance to intergranular corrosion (IGC) and stress corrosion cracking (SCC).[20,54]

Dislocation density

Figure 11*a*, *b* shows the dislocation structure within the grains and subgrains of 8090 alloy in the peak aged (T8) and 8090R280IA tempers. Figure 11*a* shows a fairly uniform distribution of dislocations inside the grains. Figure 11*b* exhibits a decrease in dislocations in the grains, compared to the original dislocations in the T8 temper. Some of the dislocations are decorated with fine precipitates, presumably formed during aging and RRA. This is quite natural, as the retrogression treatment at temperatures 280 and 250°C annihilates dislocations of opposite sign. Thus, retrogression treatment results in a decreased dislocation density. Similar observations are also reported in the literature[11,19,29] for aluminium base alloys.

Conclusions

1. Retrogression treatments cause a decrease in hardness, which is attributed to the dissolution of matrix strengthening δ' precipitates and reduction in dislocation densities. Reaging the retrogressed state results in restoration of the original peak aged hardness.
2. XRD and TEM studies show that retrogression causes dissolution of δ' phase and reaging the retrogressed state causes reprecipitation of δ' phase in the matrix.
3. RRA treatments result in generation of more dislocation loops and helices and decoration of precipitates on them. TEM photomicrographs also show widespread precipitation of S′ and T_1 precipitates on dislocations, and larger equilibrium δ precipitation along grain boundaries as well as on subgrain boundaries. In the RRA tempers, the size and distribution of δ' and β' phases are more or less the same as in the T8 temper.

Acknowledgements

The authors gratefully acknowledge the help of Mr Samar Das, National Metallurgical Laboratory, Jamshedpur with TEM studies. The authors would like to thank Dr A. A. Gokhale and Dr Vijaya Singh, Defence Metallurgical Research Laboratory, Hyderabad, India for providing the aluminium–lithium alloy.

References

1. J. R. DAVIS and DAVIS ASSOCIATES (eds) 'ASM specialty handbook, aluminum lithium alloys', 1989, Ohio, ASM International.
2. S. J. HARRIS, B. NOBLE and K. DINSDALE: Proc. 2nd Int. Conf. on

'Aluminium–lithium alloys', (ed. T. H. Sanders, Jr and E. A. Starke, Jr), 219–235; 1983, Warrendale, PA, TMS-AIME.
3. L. CHRISTODOULOU, L. STRUBLE and J. R. PICKENS: Proc. 2nd Int. Conf. on 'Aluminium–lithium alloys II', (ed. T. H. Sanders, Jr and E. A. Starke, Jr), 561–579; 1983, Warrendale, PA, TMS-AIME.
4. N. J. H. HOLROYD, A. GRAY, G. M. SCAMANS and R. HERMANN: Proc. 3rd Int. Conf. on 'Aluminium-lithium alloys III', (ed. C. Baker *et al.*), 310–320; 1985, London, The Institute of Metals.
5. F. BINSFELD, M. HABASHI, J. GALLAND, J. P. FIDELLE, D. MIANNAY and P. ROFIDAL: Proc. 4th Int. Conf. on 'Aluminium-lithium alloys IV', (ed. G. Champier *et al.*), Paris, June 1987, *J. de Phys. Colloque*, 1987, **48**, C3:587–596.
6. B. CINA: Pat. 3856584, US Patent Office, Washington, DC, December 24, 1974.
7. B. CINA and B. RANISH: Paper No. XXV, Aluminium Industrial Products, ASM, Pittsburgh, PA, USA, October 1974.
8. K. RAJAN, W. WALLACE and J. C. BEDDOES: *J. Mater. Sci.*, 1982, **17**, 2817–2824.
9. N. C. DANH, K. RAJAN and W. WALLACE: *Metall. Trans. A*, 1983, **14A**, 1843–1850.
10. M. U. ISLAM and W. WALLACE: *Met. Technol.*, 1983, **10**, 386–392.
11. V. KOMISAROV, M. TALIANKER and B. CINA: *Mater. Sci. Eng. A*, 1996, **A221**, 113–121.
12. M. KANNO, I. ARAKI and C. QUI: *Mater. Sci. Technol.*, 1994, **10**, 599–603.
13. P. J. GREGSON and H. M. FLOWER: *J. Mater. Sci. Lett.*, 1984, **3**, 829–834.
14. S. MIYASATO and G. THOMAS: Proc. 5th Int. Conf. on 'Aluminium–lithium alloys V', (ed. T. H. Sanders, Jr and E. A. Starke, Jr), 633–640; 1989, Warley, UK, Materials Component Engineering Publications Ltd.
15. P. J. GREGSON, H. M. FLOWER, C. N. J. TITE and A. K. MUKHOPADHYAY: *Mater. Sci. Technol.*, 1986, **2**, 349–353.
16. R. C. WATKINSON and J. W. MARTIN: *Mater. Charact.*, 1994, **33**, 11–19.
17. K. S. KUMAR, S. A. BROWN and J. A. PICKENS: *Acta. Mater.*, 1996, **44**, 1899–1915.
18. W. S. MILLER, J. WHITE and D. J. LLOYD: Proc. 4th Int. Conf. on 'Aluminium-lithium alloys IV', (ed. G. Champier *et al.*), Paris, June 1987, *J. de Phys. Colloque*, 1987, **48**, C3:131–149.
19. C. THAKUR and R. BALASUBRAMANIAM: *Acta Mater.*, 1997, **45**, 1323–1332.
20. Z. Q. HU, Y. ZHANG, Y. L. LIU and Z. Y. ZHU: *Corrosion*, 1993, **20**, 491–498.
21. O. JENSRUD and N. RYUM: *Mater. Sci. Eng.*, 1984, **64**, 229–236.
22. S. FOX, H. M. FLOWER and D. C. MCDARMAID: Proc. 3rd Int. Conf. on 'Aluminium–lithium alloys III', (ed. C. Baker *et al.*), 263–272; 1985, London, The Institute of Metals.
23. M. B. HALL and W. MARTIN: *Z. Metallkd.*, 1994, **85**, 134–139.
24. W. WALLACE, J. C. BEDDOES and M. C. DE MALHERBE: *Can. Aeron. Space J.*, 1981, **27**, 222–232.
25. J. K. PARK: *Mater. Sci. Eng. A*, 1988, **A103**, 223–131.
26. B. S. KANEKO: *Met. Prog.*, 1980, **118**, 41–43.
27. R. E. RICKER, J. L. FINK and A. K. VASUDEVAN: *Metall Trans. A*, 1993, **22A**, 264–267.
28. C. P. BLANKENSHSHIP JR and E. A. STARKE JR: *Metall Trans. A*, 1993, **24A**, 833–841.
29. M. TALIANKER and B. CINA: *Metall Trans. A*, 1989, **20A**, 2087–2092.
30. A. K. VASUDEVAN and R. D. DOHERTY: *Acta Met.*, 1987, **35**, 1193–1219.
31. K. SATYAPRASAD, A. A. GOKHALE, A. A. MUKHOPADHYAY, D. BANERJEE and D. B. GOEL: *Acta Mater.*, 1999, **47**, 2581–2592.
32. P. GOMIERO, F. LIVET, Y. BRECHET and F. LOUCHET: *Acta. Metall. Mater.*, 1992, **40**, 847–855.
33. A. K. GUPTA, P. GAUNT and M. C. CHATURVEDI: *Philos. Mag.*, 1987, **55**, 375–387.
34. K. SATYAPRASAD, A. K. MUKHOPADHYAY, D. BANERJEE and D. B. GOEL: *Scr. Metall.*, 1994, **30**, 1299–1304.
35. S. ABIS, E. EVANGELISTA, P. MENGUCCI and G. RIONTINO: Proc. 5th Int. Conf. on 'Aluminium-lithium alloys V', (ed. T. H. Sanders, Jr and E. A. Starke, Jr), 681–690; 1989, Warley, UK, Materials Component Engineering Publications.
36. N. RYUM: *Acta Metall.*, 1969, **17**, 269.
37. H. M. FLOWER and P. J. GREGSON: *Mater. Sci. Technol.*, 1987, **3**, 81–90.
38. E. NES: *Acta Metall.*, 1972, **20**, 499.
39. F. W. GAYLE and J. B. VANDERSANDE: *Scr. Metall.*, 1984, **18**, 473–478.
40. F. W. GAYLE and J. B. VANDERSANDE: Proc. 3rd Int. Conf. on 'Aluminium–lithium alloys III', (ed. C. Baker *et al.*), 376–385; 1985, London, The Institute of Metals.
41. F. W. GAYLE and J. B. VANDERSANDE: Proc. Int. Conf. on 'Aluminium alloys – their physical and mechanical properties', (ed. E. A. Starke and T. H. Sanders), Vol. II, 727; 1986, Warley, Engineering Materials Advisory Service.
42. E. E. UNDERWOOD: in 'Quantitative stereology', (ed. M. Cohen), 178; 1970, Reading, MA, Addison-Wesley.
43. V. RADMILOVIC, G. THOMAS, G. J. SHIFLET and E. A. STARKE JR.: *Scr. Metall.*, 1989, **23**, 1141–1146.
44. P. GOMIERO, Y. BRECHET, F. LOUCHET, A. TOURABI and B. WACK: *Acta Mater. Metall.*, 1992, **40**, 847–855.
45. C. W. LORIMER: in 'Precipitation processes in solids' (ed. K. C. Russel and H. I. Aronson), 78; 1978, Warrendale, PA, TMS.
46. R. N. WILSON and P. G. PARTRIDGE: *Acta Metall.*, 1965, **13**, 1321–1327.
47. P. GOMIERO, Y. BRECHET, F. LOUCHET, A. TOURABI and B. WACK: *Acta Mater Metall.*, 1992, **40**, 863–871.
48. K. S. GHOSH: PhD thesis, Indian Institute of Technology, October 2002.
49. S. CARESARA, A. GIARDA and A. SANCHEZ: *Philos. Mag.*, 1977, **35**, 97.
50. S. F. BAUMANN and D. B. WILLIAMS: *Metall Trans.A*, 1985, **16A**, 1203.
51. H. SUZUKI, M. KANNO and N. HAYASHI: *J. Jpn. Inst. Light Met.*, 1981, **31**, 122.
52. V. KOMISAROV, M. TALIANKER and B. CINA: *Mater. Sci. Eng. A*, 1998, **A242**, 39–49.
53. M. H. TOSTEN, A. K. VASUDEVAN and P. R. HOWELL: in Ref. 4, 490–495.
54. A. GRAY: in Proc. 4th Int. Conf. on 'Aluminium-lithium alloys IV', (ed. G. Champier *et al.*), *J. Phys. Colloq.*, 1987, **48**, C3:891–904.